American Mineralogist, Volume 91, pages 1412–1424, 2006

Stornesite-(Y), (Y, Ca)$\square_2$Na$_6$(Ca,Na)$_8$(Mg,Fe)$_{43}$(PO$_4$)$_{36}$, the first terrestrial Mg-dominant member of the fillowite group, from granulite-facies paragneiss in the Larsemann Hills, Prydz Bay, East Antarctica

Edward S. Grew,[1,*] Thomas Armbruster,[2] Olaf Medenbach,[3] Martin G. Yates,[1] and Christopher J. Carson[4]

[1]Department of Earth Sciences, University of Maine, 5790 Bryand Research Center, Orono, Maine 04469-5790, U.S.A.
[2]Laboratorium für chemische und mineralogische Kristallographie, Universität Bern, Freiestrasse 3, CH-3012 Bern, Switzerland
[3]Institut für Geowissenschaften/Mineralogie, Ruhr-Universität Bochum, D-44780 Bochum, Germany
[4]Geoscience Australia, GPO Box 378, Canberra ACT 2601, Australia

Abstract

Stornesite-(Y), end-member formula Y$\square_2$Na$_6$(Ca$_5$Na$_3$)Mg$_{43}$(PO$_4$)$_{36}$, is a new Y-dominant analog of the meteoritic mineral chladniite. A representative electron microprobe analysis is SiO_2 = 0.02, P_2O_5 = 48.11, SO_3 = 0.05, MgO = 23.16, MnO = 0.24, FeO = 15.55, Na_2O = 5.04, CaO = 5.66, SrO = 0.02, Y_2O_3 = 1.43, Yb_2O_3 = 0.24, UO_2 = 0.01, Sum = 99.53 wt%, which gives $Y_{0.68}Yb_{0.06}Na_{8.69}Ca_{5.40}Sr_{0.01}Mg_{30.71}Fe_{11.56}Mn_{0.18}Si_{0.02}S_{0.04}P_{36.22}O_{144}$. Overall, Y + REE range from 0.542 to 0.985 atoms per formula, and atomic Mg/(Mg + Fe) ratio from 0.684 to 0.749. Single-crystal X-ray diffraction gives trigonal symmetry, $R\overline{3}$, a = 14.9628(27) Å, c = 42.756(11) Å, V = 8290(4) Å^3, calculated density = 3.196 g/cm^3, Z = 3. The mineral is isostructural with synthetic chladniite, but the (0, 0, 0) site is dominantly occupied by Y instead of Ca. Bond lengths are considerably shorter than for Ca sites; Y and Yb are fully ordered at this site, which is our rationale for recognizing stornesite-(Y) as a distinct species. The strongest lines in the powder pattern [d in Å, (I), (hkl)] are 3.67 (40) (0 3 6, 3 0 6), 3.52 (40) (0 0 12, 3 1 2, 1 3 $\overline{2}$), 2.94 (60) (0 1 14, 3 2 $\overline{2}$, 2 3 2), 2.73 (100) (2 0 14, 0 3 12, 3 0 12), 1.84 (40) (1 5 14, 5 1 $\overline{14}$, 0 6 12, 6 0 12). The mineral is optically uniaxial +, n_ω = 1.6215(10) and n_ε = 1.6250(10) at 589 nm. Its color is pale yellow in standard thin sections. Stornesite-(Y) is found as inclusions in fluorapatite nodules in two paragneiss specimens from Johnston Fjord, Stornes Peninsula (whence the name) and in a third from Brattnevet, Larsemann Hills. Associated minerals are wagnerite, xenotime-(Y), monazite-(Ce), P-bearing K-feldspar, biotite, sillimanite, quartz, and pyrite; it is commonly altered to rusty material and secondary phosphates. Grains are anhedral, subhedral, or locally euhedral with hexagonal or rhombic outlines; maximum dimensions are 1 × 0.25 mm. It is inferred to have formed at 800–860 °C, 6–7 kbar by reaction of biotite with an anatectic melt locally enriched in P by interaction with fluorapatite.

Keywords: Phosphate, new mineral, Antarctica, Larsemann Hills, electron microprobe, crystal structure, granulite facies, anatexis

Introduction

The fillowite group comprises complex anhydrous phosphates that have been distinguished on the relative dominance of the divalent cations Mg, Ca, Mn, and Fe (Table 1). The Mg-dominant member, chladniite, has been found only in two meteorites. We report from a terrestrial environment a second Mg-dominant member, stornesite-(Y), that differs from chladniite in that Y is the dominant cation in a site occupied by Ca in a synthetic analog of chladniite (Domanskii et al. 1983) and by Mn and Ca in fillowite (Araki and Moore 1981; Ma et al. 2005) and its synthetic Ca-free analog (Keller et al. 2001). Like chladniite, stornesite-(Y) is a high-temperature mineral. It is found in a metamorphic environment, and its formation appears to be related closely to anatectic melts. The mineral and name were approved by the Commission on New Minerals and Mineral Names, International Mineralogical Association (2005-040). The name is for the locality, Stornes Peninsula, the westernmost major exposure in the Larsemann Hills, and for the dominance of Y at one site. Holotype material (sample no. 113002A) is deposited in the National Museum of Natural History (Smithsonian Institution) as catalog number NMNH 174436.

Occurrence

Stornesite-(Y) has only been found enclosed in fluorapatite segregations in biotite-quartz-plagioclase paragneiss, a distinctive lithologic unit characterized by segregations of cordierite, prismatine, grandidierite, and tourmaline in the Larsemann Hills, which are coastal exposures on Prydz Bay, East Antarctica (Carson et al. 1995; Ren et al. 2003). The holotype specimen (113002A and 113002AA) and specimen 113002C were collected at 69° 24.929' S, 76° 03.990' E about 200 m southwest of the south end of Johnston Fjord and 170 m north of Tassie Tarn on Stornes Peninsula (Fig. 1), the third specimen (121401E) at 69° 24.437' S, 76° 15.057' E on Brattnevet Peninsula, about 7 km east of the type locality. The holotype specimen is a rounded nodule of

* E-mail: esgrew@maine.edu

TABLE 1. Minerals of the fillowite group (Strunz and Nickel 2001) and related synthetic compounds

Mineral	End-member formula for type	Type locality/locality	Environments	Principal sources
Y or REE dominant at (0,0,0); Ca > Na at Ca1 and Ca2‡; Mg dominant at Mg1-9 and Fe10‡				
Stornesite-(Y)	$Y\square_2Na_6(Ca_5Na_3)Mg_{43}(PO_4)_{36}$*	Larsemann Hills, East Antarctica	Fluorapatite nodules in metamorphic rock	This study
Ca dominant at (0,0,0); Ca = Na or Ca > Na at Ca1 and Ca2; Mg dominant at Mg1-9 and Fe10				
Chladniite	$CaNa_8(Ca_4Na_4)Mg_{43}(PO_4)_{36}$	Carlton (IIICD) meteorite	Meteorites	McCoy et al. (1994); Floss (1999)
Synthetic	$Ca\square_2Na_6(Ca_6Na_2)CaMg_{42}(PO_4)_{36}$*			Domanskii et al. (1983)
Synthetic	$CaNa_8(Ca_4Na_4)Ca_7Cd_{12}Mg_{24}(PO_4)_{36}$,			Antenucci et al. (1996);
Synthetic	$CaNa_8(Ca_4Na_4)Ca_7Mn_{12}Mg_{24}(PO_4)_{36}$			Hatert and Fransolet (2003)
Mn or Ca dominant at (0,0,0); Ca = Na at Ca1 and Ca2; Mn dominant at Mg1-9 and Fe10				
Fillowite	$MnNa_8(Ca_4Na_4)Mn_{43}(PO_4)_{36}$*	Branchville, Connecticut	Granite pegmatites	Brush and Dana (1879, 1890); Fisher (1965); Araki and Moore (1981); Moore (1989); Fransolet et al. (1998); Ma et al. (2005)
Synthetic	$CaNa_8(Ca_4Na_4)CaMn_{42}(PO_4)_{36}$,			Hatert (2002);
Synthetic	$CaNa_8(Ca_4Na_4)Ca_7Mn_{36}(PO_4)_{36}$			Hatert and Fransolet (2003)
Ca dominant at (0,0,0); Ca > Na at Ca1 and Ca2; Fe dominant at Mg1-9 and Fe10				
Johnsomervilleite	$Ca\square_2Na_6(Ca_6Na_2)Fe_{43}(PO_4)_{36}$	Loch Quoich, Scotland	Nodule in metamorphic rock; meteorites; granite pegmatites	Livingstone (1980); Fransolet et al. (1998); Olsen et al. (1999); Sugiura and Hoshino (2003)
Mn dominant at (0,0,0); Mn = Na at Ca1 and Ca2; Mn dominant at Mg1-9 and Fe10				
Synthetic	$MnNa_8(Mn_4Na_4)Mn_{43}(PO_4)_{36}$§†			Keller et al. (2001); Hatert (2002); Hatert and Fransolet (2003)
Synthetic	$MnNa_8(Mn_4Na_4)Mg_{12}Mn_{31}(PO_4)_{36}$			Hatert and Fransolet (2003)
Fe dominant at (0,0,0); Fe = Na, K at Ca1 and Ca2; Fe dominant at Mg1-9 and Fe10				
Galileiite	$FeNa_8(Fe_4Na_4)Fe_{43}(PO_4)_{36}$	Grant IIIB meteorite	Meteorites	Olsen and Steele (1997); Olsen et al. (1999); Sugiura and Hoshino (2003)
unnamed	$FeK_8(Fe_4Na_4)Fe_{43}(PO_4)_{36}$ (?)	Sandtown IIIB meteorite	Meteorites	Olsen et al. (1999)
Ca or Na dominant at (0,0,0); Na > Ca or Mn at Ca1 and Ca2; trivalent cations present at Mg1-9 and Fe10				
Fillowite	$CaNa_8(Ca_3Na_5)Mn_{42}Fe^{3+}(PO_4)_{36}$†	Midnight Owl Mine, Arizona	Granite pegmatite	London and Burt (1982)
Synthetic	$NaNa_8(Mn_{1.2}Na_{6.8})Mn_{36.3}Fe^{2+}_{2.9}Fe^{3+}_{3.8}(PO_4)_{36}$§†			Hatert (2002); Hatert and Fransolet (2003)
Synthetic	$NaNa_8(Na_8)Na_7Cd_{24}Sc_{12}(PO_4)_{36}$			Hatert and Fransolet (2003)

* Crystal structure refinement.
† Original formula has been idealized so that cations total 96 and positive charges, 288.
‡ Occupancy for sites considered together; site labels are given in column 3, Table 5.
§ The structure has been refined, but details have not yet been published; H_2O is reported in $MnNa_8(Mn_4Na_4)Mn_{43}(PO_4)_{36}$.

dark-brown fluorapatite, ~8–10 cm across. The nodule is rimmed by a discontinuous mantle of wagnerite, which is also present in the surrounding gneiss, together with minor apatite. Specimen 113002C is from a quartz veinlet up to 10 cm thick containing subordinate plagioclase and fluorapatite segregations up to 3 cm across. Specimen 121401E is from a quartz mass not exceeding 10 cm in thickness and extending about 3 m. This mass contains fluorapatite segregations up to 5 cm across, subordinate biotite and plagioclase. Orthopyroxene is found in one thin section, in quartz adjacent to a fluorapatite segregation.

Stornesite-(Y) grains are anhedral, subhedral, or locally euhedral; subequant to elongate; subhedral and euhedral grains show hexagonal outlines (Fig. 2) or rhombic with maximum dimensions of 1×0.25 mm. The grains occur individually or in sinuous aggregates consisting of grains linked end to end; these aggregates are 0.10–0.35 mm wide and up to 3 mm long (Fig. 3). Stornesite-(Y) occurs either by itself or in association with silicates, in which case it surrounds a silicate aggregate, such as microperthitic K-feldspar (Fig. 4) or biotite and quartz (Figs. 2b and 5).

Stornesite-(Y) is commonly altered to Fe oxide and Ca-Na-Mg-Fe phosphates (Table 2; Figs. 4a and 6), or intersected by trails of very fine secondary minerals (Fig. 3). Secondary fluorapatite forms microveinlets and patches in the coarse-grained fluorapatite or on its margins. The secondary fluorapatite is fine-grained and riddled with inclusions. Monazite-(Ce) and xenotime-(Y) appear in pseudomorphs after stornesite (Y) and as fine particles in secondary fluorapatite.

PHYSICAL AND OPTICAL PROPERTIES OF STORNESITE-(Y)

Most physical properties cannot be determined because of the small grain size and the very limited amount of available material, i.e., only a few crystals exclusively in thin sections. Cleavage was not evident in thin section. The tenacity is brittle. The density calculated from the empirical formula is 3.196 g/cm^3.

Stornesite-(Y) is transparent, uniaxial (+), with n_ω = 1.6215(10) and n_ε = 1.6250(10) (λ = 589 nm). Dichroism was not observed. The color is pale yellow in thin sections of standard thickness (~0.03 mm), the same as the host fluorapatite.

CRYSTALLOGRAPHIC PROPERTIES

Powder X-ray diffraction (XRD) data were obtained with a 57.3 mm diameter Gandolfi camera and Cu$K\alpha$ radiation (Table 3) at the Ruhr-University.

Single-crystal X-ray studies were carried out with a 3-circle SMART BRUKER CCD 1K at the University of Bern, graphite-monochromated Mo$K\alpha$ radiation. The

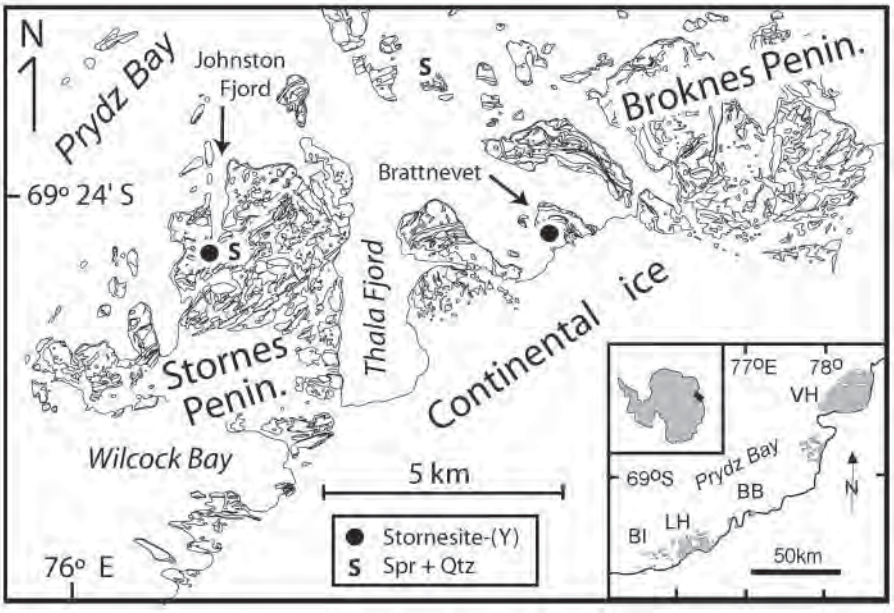

FIGURE 1. Map of the Larsemann Hills showing the localities for stornesite-(Y) and sapphirine + quartz; the locality of sapphirine + quartz near Johnston Fjord was described by Tong and Liu (1997). BI = Bolingen Islands, LH = Larsemann Hills, BB = Brattstrand Bluffs, VH = Vestfold Hills. The index map showing an outline of Antarctica and the coast of Prydz Bay was prepared by C.J.L. Wilson.

TABLE 2. Minerals enclosed in fluorapatite

Sample No.	113002A*	113002AA§	113002C	121401E
Locality	Type	Type	Type	Brattnevet
Associated with stornesite-(Y)				
Stornesite-(Y) (Sto)	x	x	x	x
Fluorapatite (Ap)	host	host	host	host
Wagnerite (Wag)	x	x	x	x
Quartz (Qz)	–	x	x	x
K-feldspar (Kfs)	–	x	x	x
Biotite (Bt)	–	–	x	x
Cordierite (?)	–	–	x	–
Sillimanite (Sil)	–	–	x	–
Monazite-(Ce) (Mnz)	x	x	x	x
Xenotime-(Y) (Xnt)	x	x	x	x
Pyrite (Py)	x	–	x	–
Not with stornesite-(Y)				
Plagioclase	–	–	–	x
Hercynite (Hc)	–	–	–	x
Magnetite (Mgt)	x	–	–	x
Ilmenite ("pseudorutile") (Ilm)	–	–	–	x
Mg-dominant sarcopside†	–	–	–	x
Secondary only				
Chlorite	–	–	x	x
Muscovite	–	–	x	–
Fluorapatite (veins and margins)	x	x	x	x
Mg-dominant wicksite‡	x	–	–	–
Mélonjosephite	x	–	–	–
Jahnsite-like	x	–	–	–
Isokite-like	–	–	x	x
Unid. Ca-Mg-Fe phosphate	x	–	–	–
Lazulite/souzalite-like	x	x	x	x
Cassiterite	x	–	–	–
Celestine	–	–	–	x

Notes: x = present.
* Holotype specimen: core of fluorapatite nodule.
† New mineral (IMA 2006-004, approved).
‡ New mineral (IMA 2005-051, approved).
§ Holotype specimen: margin of fluorapatite nodule.

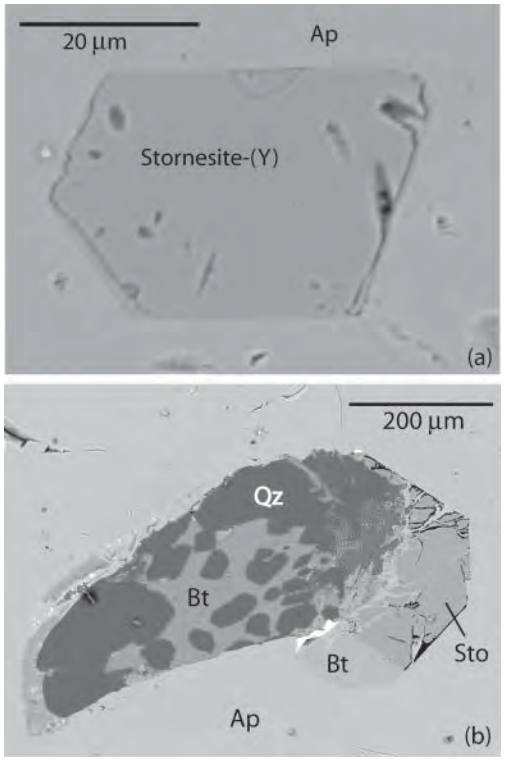

FIGURE 2. Back-scattered electron images (BSE) of euhedral stornesite-(Y) in sample 113002C (**a**) and sample 121401E (**b**). Biotite (Bt) is sieved with quartz (Qz).

studied crystal (0.07 × 0.05 × 0.03 mm) was excavated from a standard petrographic thin section using a micro-milling cutter (Medenbach 1986) and was for this reason strongly strained. Small crystal size and poor diffraction quality required an exposure time of 5 min per frame (Table 4). The structure was solved by direct methods in space group $R\bar{3}$. After it became evident that the new mineral represented a structural analog of the synthetic compound $Ca_8Na_8Mg_{42}(PO_4)_{36}$ (Domanskii et al. 1983), the atom labeling system of those authors was adopted. The structure was refined with the program SHELXL (Sheldrick 1993) including occupancies for all non-tetrahedral cation sites. Pairs of scattering factors, Mg-Fe and Na-Ca, were assigned for site occupancy refinement, depending on coordination number and average bond lengths. At this step it was recognized that the octahedral cation position at (0, 0, 0) displayed considerably higher scattering power than initially assumed. Given the electron microprobe analyses for sample 113002A (see below), 0.01 Yb (equivalent to 0.06 Yb per 144 O) was assigned as fixed constituent at this site and ratios of Y and Ca were varied to fill this Y2 position. Data quality did not allow to perform a full anisotropic refinement and therefore only O sites and selected cation positions (Ca1, Y2, Na1, and Ca2) were refined with anisotropic

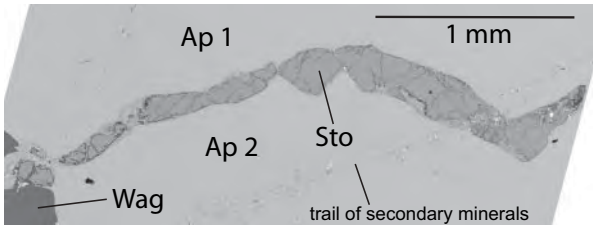

FIGURE 3. Composite assembled from BSE images of stornesite-(Y) aggregate between two fluorapatite grains in sample 113002A. The diagonal band is a trail of secondary minerals including monazite-(Ce) and xenotime-(Y). Abbreviations are given in Table 2.

TABLE 3. X-ray powder-diffraction pattern of stornesite-(Y)

I_{est}	d_{meas} (Å)	I_{calc}	d_{calc} (Å)	*hkl*
40	3.67	69.9	3.6937	0 3 6 / 3 0 6
40	3.52	25	3.5630	0 0 12
		54	3.5441	3 1 2 / 1 3 $\bar{2}$
10	3.18	6.4	3.1958	3 0 9 / 0 3 9
		18	3.1002	4 0 4
60	2.94	35.4	2.9726	0 1 14
		47.4	2.9444	3 2 $\bar{2}$ / 2 3 2
100	2.73	26.7	2.7625	2 0 14
		100	2.7485	0 3 12 / 3 0 12
10	2.62	8.3	2.6388	1 3 –11 / 3 1 11
		7.5	2.6283	4 1 6 / 1 4 $\bar{6}$ / 1 4 6 / 4 1 $\bar{6}$
30	2.47	55.2	2.4937	3 3 0
10	2.33	17	2.3538	3 3 $\bar{6}$ / 3 3 6
		6.9	2.3458	2 1 16 / 1 2 –16
10	2.12	13.2	2.1276	3 4 $\bar{1}$ / 4 3 1
		11.9	2.1197	4 3 $\bar{2}$ / 3 4 2
40	1.84	13.4	1.8511	1 5 14 / 5 1 –14
		18.4	1.8469	0 6 12 / 6 0 12

Notes: Measured intensities are visual estimates. Calculated data from Lazypulverix using a = 14.9623 Å, c = 42.756 Å based on single-crystal refinement.

displacement parameters converging at R_1 = 8.6%. The relatively high R_1 value is due to the small crystal size and poor crystal quality. In particular, weak reflections [$F_{obs} < 8\sigma(F_{obs})$] with overestimated observed intensities strongly contribute (43% of the unique reflections) to the low R_1 value. In a test refinement these weak reflections were omitted and R_1 converged at R_1 = 5.0% without significant influence on structural parameters and occupancies. Results of the refinement of the full data set are given in Tables 4 and 5, and Tables 6 and 7.[1]

Stornesite-(Y) is the fifth compound in the fillowite group for which the structure has been refined (Table 1). The fillowite-group structure is composed of six independent PO_4 tetrahedra and 14 other polyhedra, in which coordination ranges from 5 to 9 (Table 5; Fig. 7). This gives a generalized formula of $M_{60}(PO_4)_{36}$ for Z = 3. Of the 3 largest sites, which are seven-, eight- or ninefold-coordinated, one is occupied by Na only, whereas Na and Ca are disordered over the other two. Araki and Moore (1981) reported a fourth large site, their Na1, but refining Na occupancy at this position with fixed displacement parameter yielded << 10% Na, which is at the limit of resolution of our data, and we conclude that this site is vacant in stornesite-(Y). Magnesium and Fe are variably ordered over the 9 smallest sites, ranging from 100% Mg at Mg3 to 55%Mg at Mg4. Two sites are distinct in being highly regular octahedral sites with their centers placed on the threefold axes. The smaller site Fe10 at (0,0,0.5) is occupied about equally by Fe and Mg in stornesite-(Y), but by Ca in the synthetic analog of chladniite (Domanskii et al. 1983) and by Mn in fillowite (Araki and Moore 1981). The larger site (Y2) at (0, 0, 0) is occupied dominantly by Y in stornesite-(Y), but by Ca in the synthetic and by Mn in fillowite. It has considerably shorter bond lengths than the other Ca sites. In stornesite-(Y), Y and Yb are fully ordered at this site, which is our rationale for recognizing stornesite-(Y) as a distinct species in the fillowite group.

[1] For a copy of Tables 6 and 7, Document item AM-06-024, contact the Business Office of the Mineralogical Society of America (see inside front cover of recent issue) for price information. Deposit items may also be available on the *American Mineralogist* web site at http://www.minsocam.org.

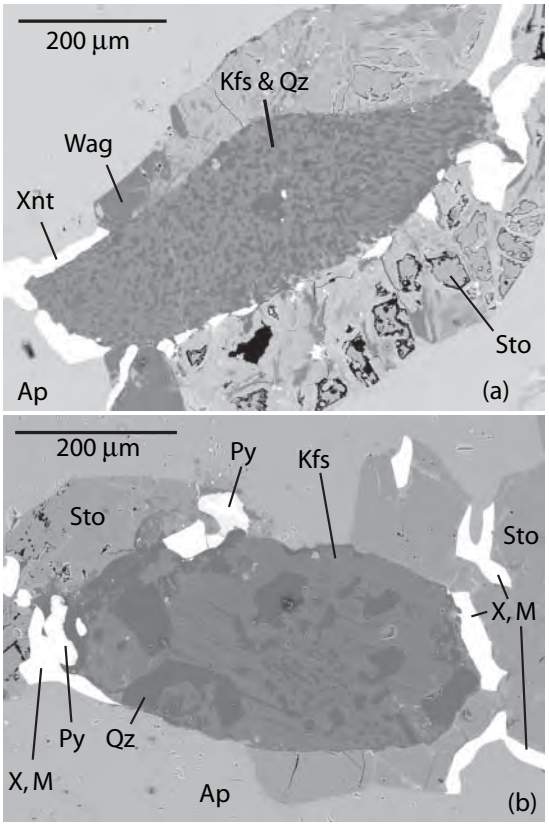

FIGURE 4. BSE images of graphic K-feldspar-quartz intergrowths in sample 113002AA (**a**) and sample 113002C (**b**). K-feldspar in **b** is microperthitic (fine dark lamellae). Stornesite-(Y) is largely altered. Only two of the white grains in **b** are pyrite (Py). X and M refer to xenotime-(Y) and monazite-(Ce); other abbreviations are given in Table 2.

TABLE 4. Details of the single-crystal X-ray structure refinement

Space group	$R\bar{3}$, No. 148
a (Å)	14.9628(27)
c (Å)	42.756(11)
V (Å^3)	8290(4)
Z	3
Calc. density (g/cm^3) empirical formula	3.196
2θ max (°)	56.30
h_{min}, h_{max}	–16, 18
k_{min}, k_{max}	–16, 19
l_{min}, l_{max}	–54, 54
Absorption correction	Empirical
R_σ	0.083
R_{int}	0.077
Parameters refined	310
Reflections meas.	16163
Unique reflections	4250
Reflections [$I > 4\sigma(I)$]	3297
R(F) [$I > 4\sigma(I)$]	0.0857
$wR(F^2)$ (all)	0.1192
$\Delta\rho_{min}$ (e/Å^3)	–1 near Mg6
$\Delta\rho_{max}$ (e/Å^3)	2 near Mg6

CHEMICAL COMPOSITION AND COMPATIBILITY INDEX OF STORNESITE-(Y)

Stornesite-(Y) and associated minerals were analyzed with a Cameca SX100 electron microprobe at the University of Maine using wavelength dispersive spectroscopy. Analytical conditions were 15 kV accelerating voltage, 10 nA beam current, and a 5 µm spot diameter for stornesite, silicates, and hercynite (except

TABLE 5. Site occupancy, coordination, and average bond lengths in stornesite-(Y)

Position labels			Site multiplicity × occupancy in stornesite-(Y)									
1	2	3	P	Fe	Mg	Ca	Na	Y	Yb	Sum	Coordination	<M-O> Å
P2	P1	P1	1.000							1.000	4	1.539
P4	P2	P2	1.000							1.000	4	1.533
P6	P3	P3	1.000							1.000	4	1.538
P3	P4	P4	1.000							1.000	4	1.539
P1	P5	P5	1.000							1.000	4	1.538
P5	P6	P6	1.000							1.000	4	1.544
Na3	Na1	Na1					1.000			1.000	7	2.528
Na2	Na2	Ca2				0.226(4)	0.107			0.333	9	2.624
Na1	–	X					0.021(4)			0.021	6	2.498
Ca	Ca1	Ca1				0.581(7)	0.419			1.000	8	2.577
M1	Ca2	Y2				0.044		0.113(1)	0.010	0.167	6	2.225
M2	Ca3	Fe10		0.085(2)	0.082					0.167	6	2.135
M3	Mg1	Mg1		0.009(3)	0.325					0.334	6	2.062
M4	Mg2	Mg2		0.011(3)	0.323					0.334	6	2.062
M5	Mg3	Mg3			0.333					0.333	6	2.096
M6	Mg4	Mg4		0.455(6)	0.545					1.000	6	2.175
M7	Mg5	Mg5		0.112(5)	0.888					1.000	6	2.122
M8	Mg6	Mg6		0.331(6)	0.669					1.000	4 + 1	2.009*
M9	Mg7	Mg7		0.280(5)	0.720					1.000	5	2.081
M10	Mg8	Mg8		0.374(5)	0.626					1.000	5	2.085
M11	Mg9	Mg9		0.208(5)	0.792					1.000	5	2.122
Sum			6.000	1.865	5.303	0.851	1.526†	0.113	0.010	15.668†		
Formula			36.000	11.190	31.818	5.106	9.156	0.678	0.060	94.008		
Wt%			48.21	15.17	24.20	5.40	5.35	1.44	0.22	100.00		

Notes: Standard deviations of refined values are given in parentheses. Labeling of positions: 1 = Araki and Moore (1981); 2 = Domanskii et al. (1983); 3 = this study.
* Four shortest bonds only.
† Does not include 0.021 Na in X site.

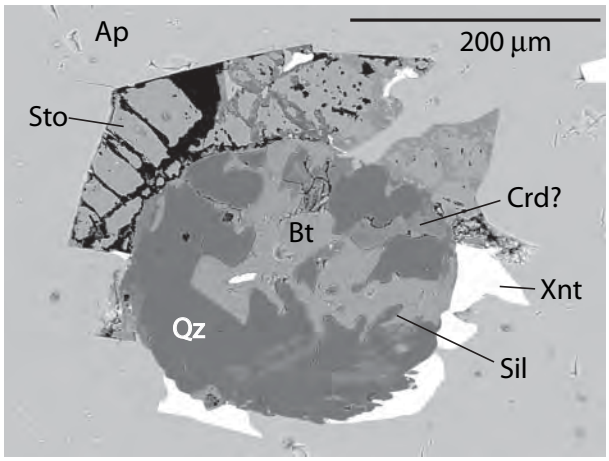

FIGURE 5. BSE image of stornesite-(Y) partially surrounding a spherical quartz-biotite aggregate in sample 113002C. One sillimanite (Sil) prism appears as a lozenge in biotite; heterogeneous material could be pinite derived from the alteration of cordierite (Crd?); other abbreviations are given in Table 2.

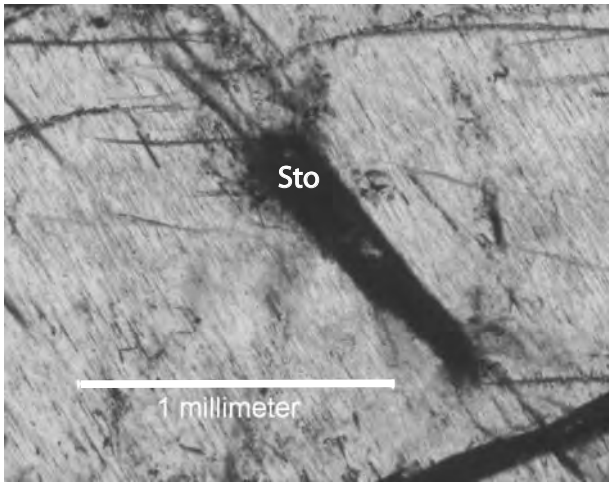

FIGURE 6. Photomicrograph of fluorapatite with acicular inclusions and highly altered stornesite-(Y). Sample 113002A. Plane-polarized light.

in a few cases where grains were so small that a focused beam had be used), and a 20 µm spot diameter for fluorapatite and wagnerite. All data were processed using the X-Phi correction of Merlet (1994). The standards used for the phosphates were fluorapatite (F*K*α), tugtupite (Na*K*α), synthetic $Mg_3(PO_4)_2$ (Mg*K*α), albite (Al*K*α), albite (Si*K*α), fluorapatite or synthetic $Mg_3(PO_4)_2$ (P*K*α), barite (S*K*α), tugtupite (Cl*K*α), fluorapatite (Ca*K*α), rutile (Ti*K*α), rhodonite (Mn*K*α), almandine (Fe*K*α), celestine (Sr*L*α), synthetic Y-Al garnet (Y*L*α), synthetic REE phosphates (REE *L*α), and U metal (U*M*β). Analyses of stornesite-(Y) are averages of 12 to 25 spots, where each constituent was counted for 5 s.

Stornesite-(Y) varies in composition from grain to grain and from sample to sample (Table 8). Magnesium and Fe vary inversely in a 1:1 ratio consistent with Mg = Fe substitution and with total Mg + Fe + Mn = 43 per 144 O (Fig. 8a). Yttrium + REE range from 0.542 to 0.985 per 144 O, almost the entire theoretically possible range for stornesite-(Y). Y is dominant among the Y + REE group and Yb is consistently present, whereas La, Ce, and Nd are present at or below the detection limits of the electron microprobe (compare chladniite, which range from HREE-enriched to LREE-enriched; Floss 1999). In terms of Ca (at Y2), Y, and Yb, compositions plot from the boundary with the chladniite field to near-complete absence of Ca at the Y site (Fig. 9). The proportions of Na, Y + REE, and Ca follow very roughly the substitution Na + (Y + REE) = 2 Ca relating the ideal stornesite-(Y) end-member (Figs. 8b and 8c) and the corresponding Y-free composition, $Ca\square_2Na_6(Ca_6Na_2)Mg_{43}(PO_4)_{36}$, which is the Mg analog of johnsomervilleite (Table 1). The scatter is most likely due to analytical uncertainties associated with the small amounts of Y and REE present and small spread in Na and Ca contents (0.8 to 1.2 atoms per 144 O for Na and Ca).

The Gladstone-Dale relation (Mandarino 1981) gives a compatibility index 1 – (K_P/K_C) = –0.030, which is excellent.

FILLOWITE GROUP: FORMULA AND NOMENCLATURE

The formula cited in most references for the fillowite group, $Na_{12}Ca_6M_{42}(PO_4)_{36}$ (e.g., Strunz and Nickel 2001), is oversimplified (see also Fransolet et al. 1998). A more appropriate formula based on structure refinements of fillowite, synthetic chladniite,

TABLE 8. Selected analyses of stornesite-(Y)

Sample	113002AA	113002A	113002C	113002C	121401E	121401E
Grain	1	2	1–2	s-2	1	3
Wt%						
SiO_2	0.25	0.02	0.05	0.10	0.29	0.25
P_2O_5	47.98	48.11	48.10	48.13	47.89	47.60
SO_3	0.03	0.05	0.02	0.03	b.d.	b.d.
MgO	23.83	23.16	24.16	23.85	23.05	21.82
MnO	0.22	0.24	0.26	0.31	0.23	0.27
FeO	15.65	15.55	14.76	14.64	16.75	17.97
Na_2O	5.09	5.04	5.45	5.18	4.72	5.08
CaO	6.07	5.66	5.26	5.76	6.10	5.89
SrO	0.03	0.02	0.00	0.01	0.01	0.02
Y_2O_3	1.10	1.43	1.85	1.51	0.97	1.12
La_2O_3	0.01	b.d.	0.01	b.d.	b.d.	0.03
Ce_2O_3	b.d.	b.d.	0.02	0.02	0.06	0.01
Nd_2O_3	n.a.	b.d.	n.a.	0.08	0.02	b.d.
Yb_2O_3	0.26	0.24	0.39	0.30	0.21	0.20
UO_2	0.02	0.01	b.d.	0.04	b.d.	b.d.
F	b.d.	0.01	0.02	b.d.	0.02	0.01
Cl	b.d.	b.d.	0.01	b.d.	b.d.	0.01
Sum	100.55	99.53	100.34	99.96	100.30	100.27
Formulae per 144 O						
Si	0.222	0.018	0.042	0.090	0.253	0.225
P	35.801	36.216	35.947	36.040	35.920	35.981
S	0.018	0.037	0.012	0.020	0.003	0
Mg	31.311	30.706	31.798	31.445	30.444	29.036
Mn	0.161	0.180	0.195	0.230	0.176	0.205
Fe	11.538	11.564	10.897	10.832	12.409	13.418
Na	8.704	8.686	9.334	8.884	8.104	8.789
Ca	5.729	5.397	4.979	5.455	5.788	5.630
Sr	0.013	0.011	0.001	0.004	0.004	0.012
Y	0.517	0.675	0.870	0.712	0.459	0.531
La	0.005	0	0.003	0	0	0.010
Ce	0	0	0.006	0.008	0.019	0.005
Nd	–	0	–	0.024	0.008	0
Yb	0.070	0.065	0.105	0.080	0.056	0.056
U	0.005	0.003	0	0.008	0	0
Sum	94.093	93.557	94.189	93.832	93.643	93.898
X_{Mg}	0.731	0.726	0.745	0.744	0.710	0.684

Notes: All Fe as FeO. Al, Ti below detection. n.a. = not analyzed; b.d. = below detection. Totals do not include F, Cl. X_{Mg} = atomic Mg/(Mg + Fe)

and stornesite-(Y) is $(Ca,Mn,Y,REE)(Na,\square)_2Na_6(Ca,Na)_8M^{2+}_{43}(PO_4)_{36}$. This formula can be generalized to $(M^{2+},Y,REE,Na)(Na,K,\square)_2(Na,K)_6(M^{2+},Na,K)_8(M^{2+},M^{3+})_{43}(PO_4)_{36}$ to include galileiite, in which Fe replaces Ca throughout, a K-dominant analog of galileiite, and several new synthetic compounds, including a Ca-free, Sc-bearing synthetic, in which Sc is presumed to occupy the M sites (Table 1). Compositions for Na-rich fillowite reported from the Midnight Owl Mine, White Picacho District, Arizona (London and Burt 1982) also can be accommodated in the more general formula if the small amount of Fe is assumed to be largely Fe^{3+}, a reasonable assumption given that natural and synthetic fillowite is reported to contain Fe^{3+} (Fransolet et al. 1998; Hatert and Fransolet 2003).

Table 1 is organized to present a provisional classification that could serve as a guide for future crystallochemical studies of the fillowite group. There are 21 cation sites in fillowite, but not all would be needed or useful in a potential classification scheme. The six tetrahedral sites and Na1 (our labeling, column 3, Table 5) are occupied by P and Na, respectively, in all structures refined to date, although a K-dominant analog of galileiite reported from the Sandtown IIIA meteorite (Olsen et al. 1999) would require partial substitution of Na by K at Na1. In contrast, the other 14 sites vary considerably in composition and have been used for recognizing different species within the fillowite group, in most cases implicitly rather than explicitly because the crystal structure was not refined in defining the species. The first criterion for recognizing different species is occupancy of the ten M sites considered together, i.e., Mg1-9 and Fe10, i.e., the dominant M cation is Mn in fillowite, Fe in johnsomervilleite, and Mg in chladniite. The second criterion is occupancy of the Ca1 and Ca2 sites considered together, which are occupied by Ca and Na in fillowite, johnsomervilleite, and chladniite, but presumably only by Fe and Na in galileiite, because no Ca was detected in the type specimen (Olsen and Steele 1997) and no more than 0.02 wt% CaO was reported in other samples (Olsen et al. 1999; Sugiura and Hoshino 2003). Keller et al. (2001) synthesized an Mn analog of galileiite. A third criterion is occupancy of the Y2 (0,0,0) site. Yttrium and REE are fully ordered at this site in stornesite-(Y), which justifies recognizing this mineral as a distinct species, the first fillowite-group mineral defined on the basis of a crystal-structure refinement. In minerals and synthetics for which the structure has not been refined, we have assumed that the (0,0,0) site is occupied preferentially by Ca relative to Mn, Fe, Cd, or Mg, so that in Table 1, Ca appears to be dominant at the (0,0,0) site except in very Mn- or Fe-rich compositions, in which these constituents are dominant instead. In any case, the (0,0,0) site might not be a useful criterion for distinguishing species when no more than a trace of Y or REE is present. A role for the often vacant X site in a classification of the fillowite group is not obvious from the compositions reported to date. Another potential criterion for recognizing distinct species is molecular H_2O, which has been found in the synthetic Mn-dominant analog of galileiite, $MnNa_8(Mn_4Na_4)Mn_{43}(PO_4)_{36}$ (Hatert and Fransolet 2003). However, attempts at specifying further criteria and developing a classification for this relatively rare mineral group are not warranted until crystallographic and compositional data on more samples have become available.

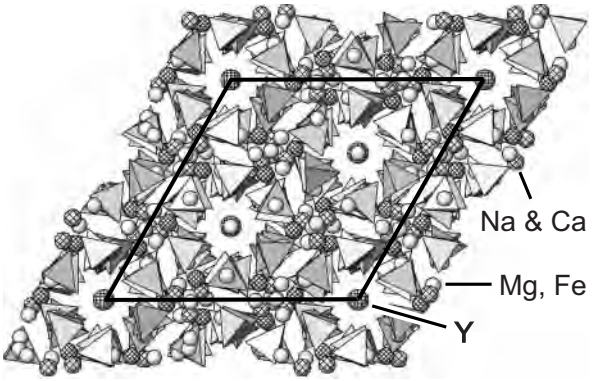

FIGURE 7. Structure of stornesite-(Y), showing PO_4 tetrahedra, Mg,Fe sites as light spheres, Na and Ca sites as cross-hatched spheres (diagonal), and the Y-rich site as cross-hatched spheres (horizontal-vertical).

We have introduced the new root name, stornesite, because chladniite is not a REE mineral, i.e., adding a Levinson modifier for REE to chladniite, e.g., "chladniite-(Y)" has no precedent. The precedent was most recently followed in naming a new mineral isostructural with agardite in the mixite group (Walenta and Theye 2005). Agardite is a REE mineral, and thus has a Levinson modifier. In the new mineral, Pb is dominant at the structural site occupied dominantly by REE in agardite, so it was not named agardite, but plumboagardite.

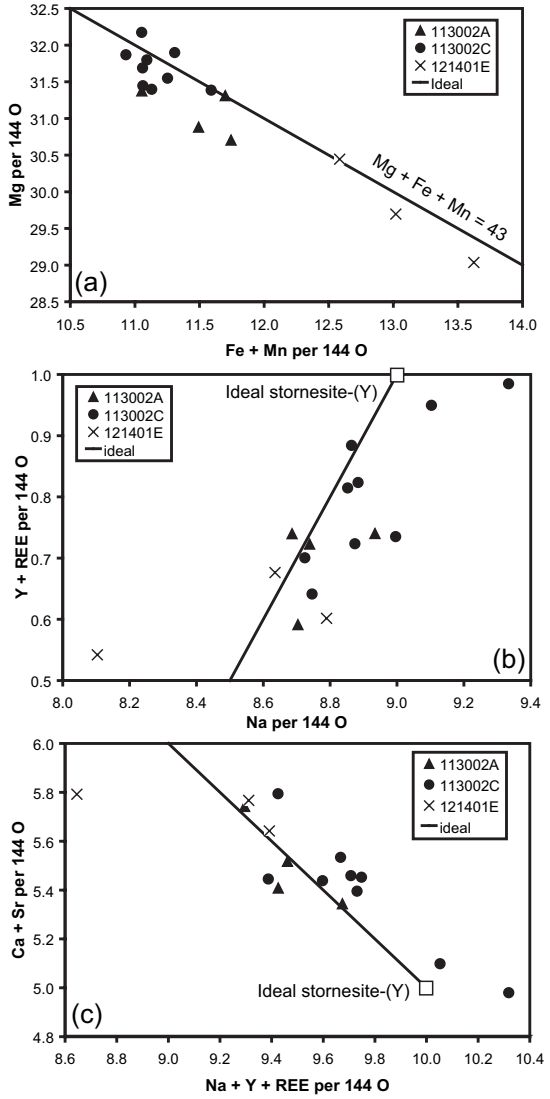

FIGURE 8. Variations in stornesite-(Y) composition from grain to grain in three samples (113002AA included with 113002A). (**a**) The line indicated as ideal indicates the substitution (Fe,Mn)Mg_{-1} in the ideal stornesite-(Y) composition. (**b** and **c**) The line indicated as ideal indicates the substitution Na(Y,REE)Ca_{-2} relating the ideal compositions for end-member stornesite-(Y) and the Mg analog of johnsomervilleite (Table 1).

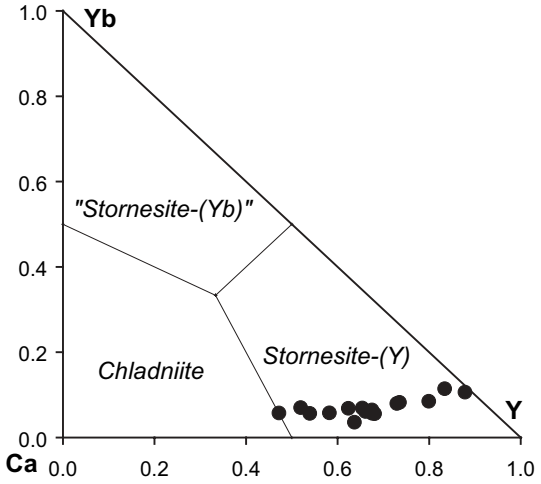

FIGURE 9. Plot of Ca (at Y2), Y, and Yb contents in stornesite-(Y) per 144 O atoms. Ca occupancy at the Y2 site is assumed to be 1 – Y – REE, i.e., compositions have been projected from REE-Yb onto the Ca-Y-Yb plane. Fields for chladniite, stornesite-(Y), and a hypothetical "stornesite-(Yb)" determined by the 50-50 rule. "Stornesite-(Yb)" is in quotation marks because no such mineral has been submitted for consideration or approved by the Commission on New Minerals and Mineral Names, International Mineralogical Association.

ASSOCIATED MINERALS

The minerals found in the stornesite-(Y)-bearing fluorapatite segregations or in the quartz masses associated with the segregations constitute a diverse suite (Table 2). Fluorapatite grains in the segregations range from 2 mm in 121401E to 4 cm across in the holotype specimen, and are anhedral; the centimeter-sized grains in the holotype specimen show cleavage. Fluorapatite in the two specimens from the type locality contain very abundant, fine acicular inclusions of Fe-sulfide parallel to **c** (Fig. 6); semi-quantitative EDS analyses give Fe/S ratios consistent with pyrite in some inclusions, with pyrrhotite in others. The fluorapatite composition (Table 9) is noteworthy for its relatively high Cl, Y_2O_3, MgO, and FeO contents, which greatly exceed the ranges reported for most metamorphic fluorapatite (Kapustin 1987; Povondra 1992; Bea and Montero 1999; Spear and Pyle 2002; Harlov and Förster 2002). The contents of REE + Y per formula unit average roughly 70% of the Na content (except for one spot unusually enriched in Yb, Table 9), that is, at less than the 1:1 ratio predicted by the substitution Na + (Y, REE) = 2Ca (Pan and Fleet 2002); Harlov et al. (2006) reported a similar deviation from stoichiometry in Si-poor, chlor- and fluorapatite from a pelitic xenoliths from the Stromboli volcano, Italy. Fluorapatite with similar FeO contents has been reported from a pegmatoid in association with almandine-rich garnet (2.22 wt% FeO, Fransolet and Schreyer 1981), orthogneiss (2.38 wt% FeO, Povondra and Vrána 1993), and from pumice (1.43–2.67 wt% FeO, Heming and Carmichael 1973); however, the chlor-fluorapatite from Stromboli is by far the richest in FeO reported to date, 4.88 wt% (Harlov et al. 2006).

In the holotype specimen, wagnerite enclosed in fluorapatite is colorless or pale yellow in thin section, in contrast to the distinctly yellow wagnerite mantling the nodule and in enclosing gneiss, as well as wagnerite found elsewhere in the biotite-quartz-plagioclase gneiss (e.g., Ren et al. 2003, 2005). Wagnerite forms subequant to elongated, anhedral to nearly euhedral grains some of which have exterior angles <180° (holotype specimen) and mostly range from 0.5 to 1 mm in length. Fluorapatite in the holotype and Brattnevet specimens also encloses wagnerite sheets generally 0.1 mm thick, but up to 1.2 cm across. In the Brattnevet specimen, pale yellow wagnerite commonly is associated with biotite enclosed in fluorapatite (Fig. 10). Analyzed pale wagnerite contains minor Fe and <0.1 wt% TiO_2 (e.g., Table 9) in contrast to yellow Ti-bearing wagnerite such as that analyzed in

TABLE 9. Selected analyses of fluorapatite (Ap) and wagnerite (Wag)

Mineral	Ap	Ap	Ap	Ap	Wag	Wag	Wag	Wag
Sample	113002A	113002AA	113002C1	121401E	113002A	121401E	112906H2*	120302C†
Grain	2	1	1	2	1	5	average	average
wt%								
SiO_2	b.d.	b.d.	b.d.	b.d.	0.02	0.03	0.03	0.02
P_2O_5	41.22	41.29	41.32	41.29	42.70	41.88	41.75	42.28
SO_3	0.16	0.04	0.11	b.d.	b.d.	n.a.	0.01	b.d.
TiO_2	0.02	b.d.	b.d.	b.d.	b.d.	0.06	0.59	0.32
Al_2O_3	b.d.	b.d.	b.d.	b.d.	b.d.	0.03	0.01	b.d.
MgO	0.63	0.95	0.73	0.71	45.01	45.17	44.79	45.60
MnO	0.20	0.23	0.21	0.25	0.10	0.11	0.08	0.06
FeO	2.81	3.12	2.57	3.23	5.83	7.10	6.26	5.66
Na_2O	0.26	0.36	0.27	0.26	n.a.	b.d.	n.a.	n.a.
CaO	50.06	48.96	50.44	49.79	0.09	0.11	0.18	0.15
SrO	0.01	0.03	b.d.	b.d.	b.d.	n.a.	0.01	b.d.
Y_2O_3	0.47	0.53	0.49	0.48	0.01	n.a.	0.01	0.01
La_2O_3	b.d.	0.14	0.07	0.14	b.d.	n.a.	0.02	b.d.
Ce_2O_3	0.15	0.35	0.19	0.25	0.03	n.a.	b.d.	b.d.
Nd_2O_3	0.12	b.d.	0.01	0.01	n.a.	n.a.	n.a.	n.a.
Tm_2O_3	0.03	n.a.	n.a.	n.a.	n.a.	n.a.	n.a.	n.a.
Yb_2O_3	0.07	1.09	0.02	0.04	n.a.	n.a.	n.a.	n.a.
UO_2	0.10	b.d.	b.d.	b.d.	n.a.	n.a.	n.a.	n.a.
F	2.12	2.05	2.32	2.27	10.01	10.57	10.38	10.21
Cl	2.09	2.47	1.98	2.05	0.01	b.d.	b.d.	b.d.
H_2O calc	0.19	0.13	0.13	0.13	0.60	0.36	0.41	0.53
O = F, Cl	–1.36	–1.42	–1.42	–1.42	–4.22	–4.45	–4.37	–4.30
Sum	99.35	100.33	99.43	99.50	100.20	100.98	100.17	100.54
Formulae								
O (anhydrous)	12.5	12.5	12.5	12.5	4.5	4.5	4.5	4.5
Si	0	0	0	0	0.001	0.001	0.001	0
P	2.997	2.998	2.996	3.001	1.000	0.983	0.984	0.988
S	0.010	0.003	0.007	0	0	–	0	0
Ti	0.001	0	0	0	0	0.001	0.012	0.007
Al	0	0	0	0	0	0.001	0	0
Mg	0.081	0.122	0.094	0.090	1.857	1.867	1.859	1.878
Mn	0.015	0.017	0.015	0.018	0.002	0.003	0.002	0.001
Fe	0.202	0.224	0.184	0.232	0.135	0.165	0.146	0.131
Na	0.044	0.059	0.045	0.044	–	0	–	–
Ca	4.606	4.500	4.628	4.581	0.003	0.003	0.005	0.005
Sr	0	0.002	0	0	0	–	0	0
Y	0.022	0.024	0.022	0.022	0	–	0	0
La	0	0.004	0.002	0.005	0	–	0	0
Ce	0.005	0.011	0.006	0.008	0	–	0	0
Nd	0.004	0	0	0	–	–	–	–
Tm	0.001	–	–	–	–	–	–	–
Yb	0.002	0.028	0	0.001	–	–	–	–
U	0	0	0	0	–	–	–	–
Sum	7.988	7.992	7.999	8.002	2.998	3.023	3.010	3.010
F	0.577	0.557	0.627	0.617	0.877	0.927	0.914	0.892
Cl	0.304	0.360	0.288	0.298	0	0	0	0
H_{calc}	0.119	0.083	0.085	0.085	0.123	0.073	0.086	0.108
Sum	1	1	1	1	1	1	1	1
X_{Mg}	0.286	0.352	0.337	0.280	0.932	0.919	0.927	0.935

Notes: n.a. = not analyzed; b.d. = below detection. All Fe as FeO. H_2O calculated from stoichiometry: F + Cl + H = 1. X_{Mg} = atomic Mg/(Mg+Fe).
* From 250 m E of type locality.
† From base of Gneiss Peak, 500 m ENE of type locality.

nodules from two nearby localities and in gneiss (Ren et al. 2003, 2005). Two wagnerite crystals in the holotype specimen are the 7*b* polytype (Table 10), whereas two wagnerite crystals in the section containing Mg-dominant sarcopside from Brattnevet, as well as wagnerite in other samples, are the 5*b* polytype (Table 10; Ren et al. 2003, 2005).

Monazite-(Ce) and xenotime-(Y) occur in a variety of textures, e.g., as selvages along grain boundaries (e.g., Figs. 4b and 5) or rods in coarse fluorapatite.

K-feldspar is in places microperthitic, and its intergrowth with quartz in specimens from the type locality suggests graphic granite, but microscopic in scale (Fig. 4). In the Brattnevet specimen, K-feldspar is commonly associated with biotite, vermicular hercynite, magnetite, and altered ilmenite ("pseudorutile") in a texture suggestive of biotite breakdown (Fig. 10). K-feldspar contains 0.09–1.09 wt% P_2O_5; plagioclase (An_{17-18}), 0.3 wt% P_2O_5 (e.g., Table 11). The EMPA data (Fig. 11) are consistent with P

TABLE 10. Wagnerite: cell parameters

Sample	113002A	113002A	112906H2*	120302C†
Polytype	*7b*	*7b*	*5b*	*5b*
a (Å)	9.6481(8)	9.6486(13)	9.659(2)	9.6542(12)
b (Å)	44.374(5)	44.364(11)	31.69(2)	31.687(7)
c (Å)	11.9191(9)	11.9208(15)	11.918(2)	11.9259(13)
β	108.289(7)°	108.31(1)°	108.26(2)°	108.25(1)°
V (Å^3)	4845.1(8)	4843(1.5)	3464(2)	3465(1)

* From 250 m E of type locality.
† From base of Gneiss Peak, 500 m ENE of type locality.

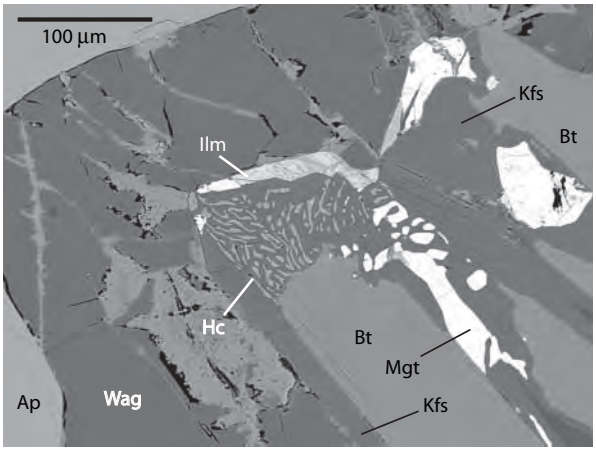

FIGURE 10. BSE image of biotite (Bt) partially replaced by vermicular hercynite (Hc), magnetite (Mgt), altered ilmenite (Ilm), and perthitic K-feldspar (Kfs), all with a wagnerite mantle (Wag) in fluorapatite (Ap) sample 121401E.

incorporation by the substitution $PAlSi_{-2}$ (London et al. 1990).

Brown biotite associated with breakdown melt textures (e.g., Fig. 10) is rich in TiO_2, F, and Cl (columns 1–2, Table 12); high totals could result from overestimating unanalyzed H_2O assuming anion stoichiometry in Ti-rich biotite (Cesare et al. 2003). Biotite sieved with quartz (Fig. 2b) or associated with sillimanite (Fig. 5) is commonly olive-green in color and contains little Ti (column 3; Table 12).

Hercynite is also present in one quartz inclusion in specimen 121401E (Fig. 12a); it contains minor Zn and V, but negligible Cr (Table 13).

ORIGIN OF STORNESITE-(Y) AND ASSOCIATED FERROMAGNESIAN PHOSPHATES

The origin of stornesite-(Y) and the distinctive suite of minerals (Ti-poor wagnerite, P-bearing K-feldspar, Mg-dominant sarcopside) found only as inclusions in fluorapatite must be considered as tied closely to the process by which fluorapatite and associated plagioclase-bearing quartz masses and veins were segregated. The presence of high-temperature mineral assemblages such as hercynite + quartz and K-feldspar + hercynite + magnetite (from biotite breakdown) in the fluorapatite suggests that the segregation process occurred at close to peak metamorphic temperatures rather than at lower temperatures during post-peak fluid activity on the retrograde path. One possibility is that the segregation process is genetically linked to anatexis, which pervasively affected the Larsemann Hills (e.g., Stüwe et al. 1989; Dirks et al. 1993; Carson et al. 1997), that is, the fluorapatite segregations and plagioclase-bearing quartz could be restitic bodies remaining after melt had been extracted, an origin Carson et al. (1997) ascribed to cordierite-bearing, quartz-plagioclase leucosomes in the Larsemann Hills. Relatively high FeO contents of apatite-group minerals have only been reported in high-temperature igneous rocks (Heming and Carmichael 1973; Fransolet and Schreyer 1981) or from pelitic xenoliths that had been partially melted and metasomatized by chloride-rich fluids (Harlov et al. 2006). The association of Fe-bearing apatite-group minerals with melts in other areas suggests that the fluorapatite

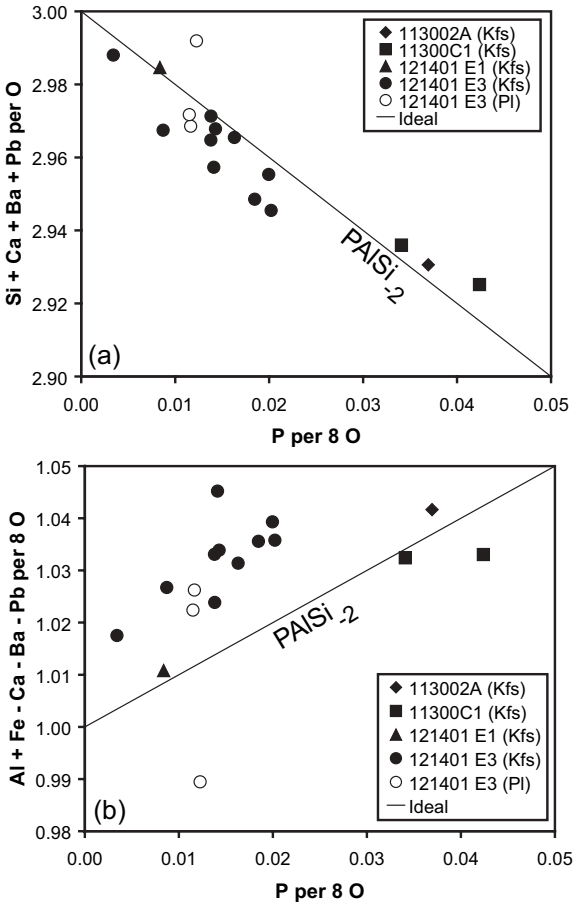

FIGURE 11. Variations in feldspar composition as a function of P content. Reference lines are shown for the idealized substitution $PAlSi_{-2}$.

nodules formed in the presence of an anatectic melt at the peak temperatures of metamorphism in the Larsemann Hills.

Permeation of the fluorapatite segregations with melt is suggested by the presence of K-feldspar-quartz intergrowths, one of which is distinctly graphic (Fig. 4); these intergrowths could be crystallized entrapped melt that was not altered on the retrograde path. Phosphorus contents up to 1 wt% P_2O_5 in K-feldspar enclosed in fluorapatite (Table 11) suggests melt P_2O_5 contents might have also reached 1 wt% had these melts been peraluminous (London 1992; London et al. 1999), a reasonable assumption given the presence of sillimanite and possible cordierite in a few inclusions. Phosphorus diffuses slowly in peraluminous granitic melts (Wolf and London 1994; London 1998), and thus, very likely it became concentrated in the melt permeating the fluorapatite nodules and did not diffuse out into the main mass of melt. By analogy with the reactions proposed by London et al. (1999), the development of wagnerite coronas around biotite with breakdown textures (Fig. 10) could be attributed to reaction of biotite with a phosphate-bearing melt:

$$Bt + P_2O_5 \text{ (in melt)} \pm \text{fluorapatite} \Rightarrow Kfs + Hc + Mgt + Ilm + \text{wagnerite}$$

TABLE 11. Selected analyses of feldspar

Sample	121401E	121401E	113002AA	113002C
Grain	Kfs 3-1-2a	Pl 1-1	Kfs	Kfs 1
Wt%				
SiO_2	63.21	63.41	63.25	63.40
Al_2O_3	18.96	22.26	19.10	18.94
P_2O_5	0.51	0.33	0.94	1.09
Fe_2O_3	0.18	0.06	0.01	0.14
MnO	b.d.	b.d.	0.01	b.d.
MgO	0.01	b.d.	0.01	0.01
Na_2O	1.54	9.16	0.59	0.89
K_2O	14.53	0.65	15.44	15.41
CaO	0.11	3.72	b.d.	0.01
BaO	0.19	b.d.	0.05	0.03
PbO	n.a.	n.a.	0.03	b.d.
Sum	99.23	99.60	99.42	99.92
Formulae per 8 O				
Si	2.937	2.815	2.929	2.924
Al	1.038	1.165	1.043	1.029
P	0.020	0.012	0.037	0.042
Fe	0.006	0.002	0	0.005
Mn	0	0	0	0
Mg	0.001	0	0	0
Na	0.139	0.788	0.053	0.080
K	0.861	0.037	0.912	0.906
Ca	0.005	0.177	0.000	0.001
Ba	0.003	0.000	0.001	0.001
Pb	–	–	0.000	0.000
Sum	5.011	4.996	4.976	4.988

Notes: All Fe as Fe_2O_3. n.a. = not analyzed; b.d. = below detection.

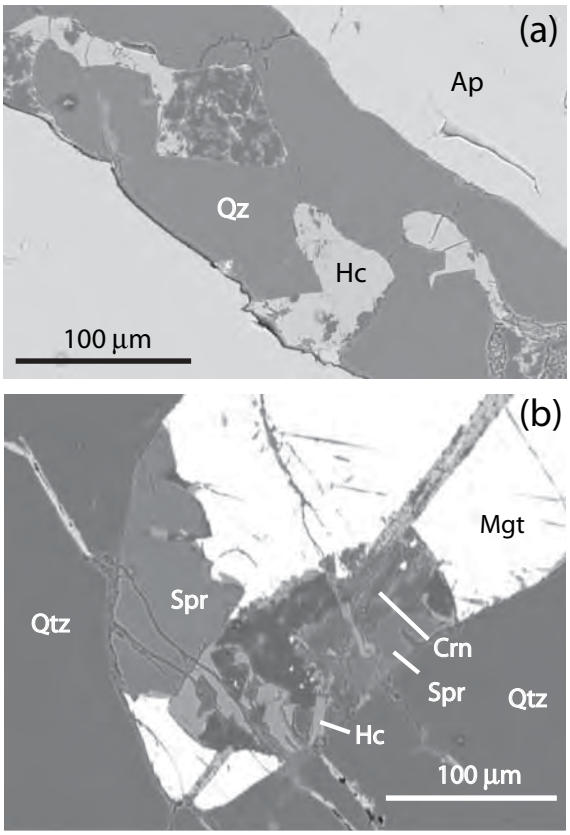

FIGURE 12. BSE images of (**a**) hercynite (Hc) in quartz (Qz) enclosed by fluorapatite (Ap); dark patches in hercynite is secondary diaspore (sample 121401E) and (**b**) sapphirine (Spr), corundum (Crn), hercynite, and magnetite (Mgt) in quartz. Paragneiss sample 112702A (unnamed island northeast of Stornes Peninsula).

TABLE 12. Selected analyses of biotite in sample 121401E

Grain	3-1-1*	3-6-2*	0-1†
Wt%			
SiO_2	35.55	36.81	36.65
P_2O_5	0.05	0.05	0.06
TiO_2	6.51	6.64	0.05
Al_2O_3	15.58	15.16	19.04
Cr_2O_3	0.06	0.11	b.d.
K_2O	9.82	9.56	9.50
Na_2O	0.10	0.13	0.02
CaO	b.d	0.04	0.02
BaO	0.17	0.14	b.d.
MgO	10.77	10.84	12.53
MnO	0.01	0.02	b.d.
FeO	16.96	17.85	16.30
F	1.01	1.11	0.93
Cl	0.64	0.63	0.76
H_2O calc	3.32	3.35	3.33
O = F, Cl	–0.57	–0.61	–0.56
Total	99.97	101.84	98.63
Formula per 22 O anhydrous			
Si	5.383	5.469	5.539
P	0.006	0.007	0.007
^{IV}Al	2.611	2.524	2.454
Sum IV	8	8	8
Ti	0.741	0.742	0.006
^{VI}Al	0.170	0.129	0.938
Cr	0.008	0.013	0
Mg	2.431	2.402	2.822
Mn	0.001	0.003	0
Fe	2.148	2.218	2.061
Sum VI	5.499	5.507	5.826
K	1.897	1.812	1.833
Na	0.029	0.038	0.005
Ca	0.000	0.006	0.004
Ba	0.010	0.008	0
Sum XII	1.936	1.864	1.841
Total cations	15.436	15.371	15.668
F	0.485	0.519	0.446
Cl	0.164	0.158	0.195
H_{calc}	3.351	3.322	3.359
Sum	4	4	4
X_{Mg}	0.531	0.520	0.578

Notes: All Fe as FeO. b.d. = below detection. H_2O calculated assuming stoichiometry: F + Cl + H = 4. X_{Mg} = atomic Mg/(Mg + Fe).
* Associated with breakdown melt textures similar to that shown in Figure 10.
† Sieved with quartz (Fig. 2b). V and Ni near limits of detection.

TABLE 13. Analysis of hercynite in sample 121401E (Fig. 12a)

	wt%	3 cat/4 O
Nb_2O_5	0.01	0
TiO_2	0.02	0
SnO_2	0.01	0
Al_2O_3	56.98	1.898
V_2O_3	0.25	0.006
Cr_2O_3	0.02	0.000
Fe_2O_3	4.43	0.094
MgO	6.05	0.255
MnO	0.03	0.001
FeO	30.76	0.727
ZnO	0.88	0.018
Total	99.43	3
X_{Mg}		0.259

Notes: Fe^{3+}/Fe^{2+} ratio calculated by stoichiometry. Ni, Ta, W below detection. X_{Mg} = atomic Mg/(Mg + Fe^{2+}).

That is, Mg and some Fe in biotite were incorporated in ferromagnesian phosphate instead of ferromagnesian silicate as in most melting reactions. In the cases where stornesite-(Y) forms coronas around K-feldspar (Fig. 4) in the absence of biotite, we infer that the permeating melt was sufficiently enriched

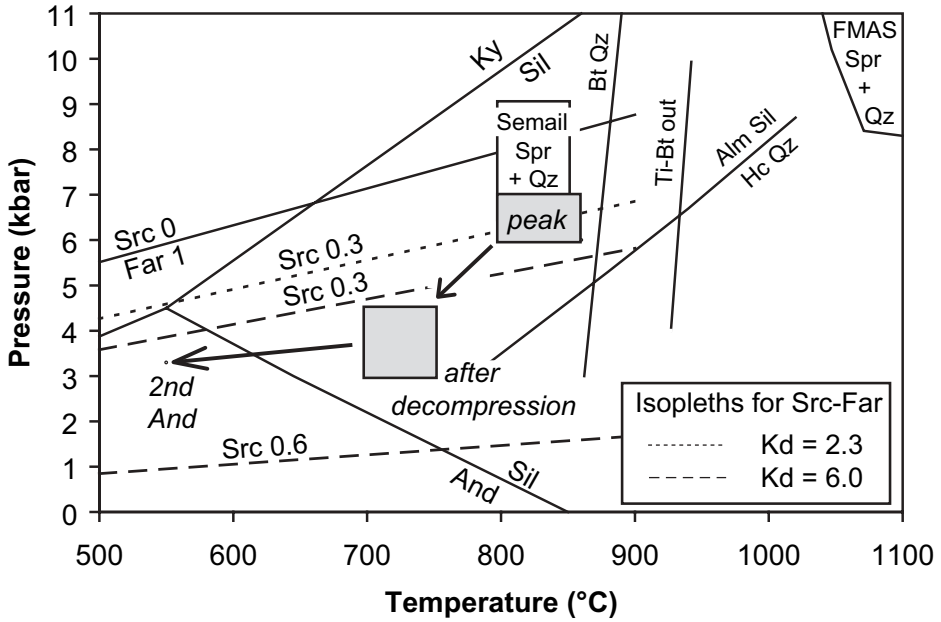

FIGURE 13. Schematic pressure-temperature diagram illustrating stability relationships relevant to the present study. Boxes and arrows indicate post-peak metamorphic evolution based on *P-T* estimates reported for the Brattstrand Bluffs coastline (Fig. 1) 10–50 km northeast of Broknes Peninsula (Fitzsimons 1996), the Larsemann Hills (Carson et al. 1997), and from the Bolingen Islands (Fig. 1) 5–15 km west and southwest of Stornes Peninsula (Thost et al. 1994). Sources of other data: Al_2SiO_5 relations (Pattison 1992); hercynite + quartz = almandine + sillimanite in experimental FeO-Al_2O_3-SiO_2 system (Holdaway and Lee 1977; Bohlen et al. 1986); estimated conditions for sapphirine + quartz in the Semail Ophiolite (Gnos and Kurz 1994); theoretical conditions for sapphirine + quartz in the FeO-MgO-Al_2O_3-SiO_2 system at low oxygen activities (Harley 1998); theoretical breakdown of biotite + quartz to melt + orthopyroxene + K-feldspar + garnet during fluid-absent partial melting of metapelites and metagraywackes (Bt Qz, Vielzeuf and Holloway 1988); experimental upper-temperature stability limit for Ti-bearing biotite + quartz during fluid-absent partial melting of metagraywackes (Ti-Bt out, Stevens et al. 1997); Mg-analog of sarcopside (Src 0)-farringtonite (Far 1) stability in the $Mg_3(PO_4)_2$ system (solid line, Brunet and Vielzeuf 1996; Brunet et al. 1998). The isopleths for sarcopside with 30 and 60% of the Fe end-member were calculated from the reaction and volume change in the $Mg_3(PO_4)_2$ system and assuming both solid solutions are ideal. $K_D = (Mg/Fe)_{Far}/(Mg/Fe)_{Src} = 2.30$ was calculated from compositions of these two minerals in association with johnsomervilleite and chladniite reported by Livingstone (1980), Černý et al. (1998), Corbella i Cordomí and Melgarejo i Draper (1990), and McCoy et al. (2006). $K_D = 6$ is the minimum value consistent with synthesis of a sarcopside with 60% Fe end-member at 500 °C, 0.8 kbar (Charalampides et al. 1988). Abbreviations from Table 2; also And = andalusite, Ky = kyanite, Spr = sapphirine.

in MgO, FeO, and P_2O_5 from interaction with fluorapatite and biotite in one part of a fluorapatite nodule for ferromagnesian phosphate to crystallize in a part lacking biotite. We also explain the more common occurrence of ferromagnesian phosphates as isolated inclusions in fluorapatite (e.g., Fig. 2a) or interstitial to fluorapatite grains (e.g., Fig. 3) as sites from which the melt had been extracted completely. The inclusions consisting of stornesite-(Y) with Ti-poor biotite, fine-grained sillimanite and cordierite(?) (Figs. 2b and 5) could be crystallized entrapped melt that was altered by the hydrous component released from the melt when it crystallized on the retrograde path (e.g., White and Powell 2002). In summary, the situation in the Larsemann Hills fluorapatite nodules is analogous to that proposed by London et al. (1999) to explain mineral assemblages with zwieselite (Fe-dominant analog of wagnerite) and sarcopside in evolved S-type granites and pegmatites.

The pressure-temperature evolution in the Larsemann Hills and nearby areas belonging to the same metamorphic complex followed a clockwise path in which peak temperatures were followed by decompression (Fig. 13). Peak conditions have been estimated to be 800–860 °C, 6–7 kbar on the basis of thermometers and barometers in pelitic, felsic, mafic, and calc-silicate granulites. Further insight on metamorphic conditions is provided by Mg-dominant sarcopside and hercynite + quartz in the Brattnevet sample and by sapphirine + quartz at two localities (Figs. 1 and 12b). The presence of Mg-dominant sarcopside with 28% of the Fe end-member agrees with inferred peak pressure conditions based on isopleths for sarcopside solid solution coexisting with farringtonite. However, sapphirine and hercynite would be stable with quartz at the inferred temperatures only under oxidizing conditions or in the presence of other components. Sapphirine + quartz formed at much lower temperatures in the Semail Ophiolite than is predicted from the FeO-MgO-Al_2O_3-SiO_2 system at low oxygen activities (Fig. 13); there it occurs with magnetite, hercynite, and ilmeno-hematite (Gnos and Kurz 1994) in a texture very similar to that in Figure 12b. Stoichiometric recalculation of the sapphirine composition reported by Tong and Liu (1997) for the locality near Johnston Fjord (Fig. 1) yields $Fe^{3+} = 0.367$ and $Fe^{2+} = 0.700$ per 14 cations/20 O, consistent with an oxidizing environment for this sample. Stability of hercynite + quartz

at the conditions inferred for the Larsemann Hills is less easily rationalized on the basis of impurities, nonetheless the amount of Fe^{3+} and Zn taken together, might be sufficient to shift the equilibrium 50–70 °C down-temperature.

Ti-rich, F- and Cl-bearing biotite within the fluorapatite segregations has only partially broken down at the peak metamorphic conditions, an observation consistent with the retention of biotite in quartz-absent assemblages in the Brattstrand Bluffs (Fitzsimons 1996) and with experimental data and petrologic grids that predict stability for Ti-rich, F- and Cl-bearing biotite under the peak conditions for the Larsemann Hills (Fig. 13).

Whether anatexis was primarily a consequence of high temperatures (e.g., Fitzsimons 1996) or of decompression (e.g., Carson et al. 1997) is a matter of debate; andalusite-bearing melts developed in fluorapatite nodules in the southern Stornes Peninsula suggest that some melting occurred during or after decompression. Nonetheless, it is likely that stornesite-(Y) formed at peak temperatures or during the earliest stages of decompression rather than at lower temperatures in the later stages. A high-temperature origin for stornesite-(Y) in the Larsemann Hills is consistent with most available information on other fillowite-group minerals; an exception is secondary fillowite in the Midnight Owl Mine (London and Burt 1982). Chladniite is known only from two meteorites; temperatures could have reached ~1050 °C, sufficient for limited silicate melting, in the chladniite-bearing GRA 95209 meteorite (Floss 2000; McCoy et al. 2006). Synthetic fillowite crystallizes above 600 °C with alluaudite in Mn-rich compositions (Hatert and Fransolet 2004), and a synthetic Cd-bearing analog of alluaudite is transformed into a Cd-bearing analog of fillowite at 850–860 °C (Antenucci et al. 1996). However, high temperatures are not the only constraint on stornesite-(Y) formation. Reaction of anatectic melts with fluorapatite and biotite play a critical role; the resulting P-enriched melt affords the precipitation of a diverse suite of ferromagnesian phosphates dominated by wagnerite, but including Mg-dominant sarcopside and stornesite-(Y).

ACKNOWLEDGMENTS

We thank the leader, Bob Jones, and other members of the 2003–2004 Australian National Antarctic Research Expedition for logistic support during the summer field season. The fieldwork of C.J.C. and E.S.G. in the Larsemann Hills was supported by Antarctic Science Advisory Committee Project no. 2350. We thank Frédéric Hatert and Sergey Britvin for their thoughtful reviews, Sergey Krivovichev for editorial handling, Chris J.L. Wilson for the index map in Figure 1, Fabrice Brunet and Christian Chopin for advice on calculating isopleths for sarcopside solid solutions. The research of E.S.G. and M.G.Y. was supported by U.S. National Science Foundation grants OPP-0228842 and MRI-0116235 to the University of Maine.

REFERENCES CITED

Antenucci, D., Tarte, P., and Fransolet, A.-M. (1996) The synthetic phosphate $NaCaCdMg_2(PO_4)_3$: first experimental evidence of a reversible alluaudite-fillowite polymorphism. Neues Jahrbuch für Mineralogie Monatshefte, 1996, 289–296.

Araki, T. and Moore, P.B. (1981) Fillowite, $Na_2Ca(Mn,Fe)^{2+}_7(PO_4)_6$: its crystal structure. American Mineralogist, 66, 827–842.

Bea, F. and Montero, P. (1999) Behavior of accessory phases and redistribution of Zr, REE, Y, Th, and U during metamorphism and partial melting of metapelites in the lower crust: An example from the Kinzigite Formation of Ivrea-Verbano, NW Italy. Geochimica et Cosmochimica Acta, 63, 1133–1153.

Bohlen, S.R., Dollase, W.A., and Wall, V.J. (1986) Calibration and applications of spinel equilibria in the system FeO-Al_2O_3-SiO_2. Journal of Petrology, 27, 1143–1156.

Brunet, F. and Vielzeuf, D. (1996) The farringtonite / $Mg_3(PO_4)_2$-II transformation: A new curve for pressure calibration in piston-cylinder apparatus. European Journal of Mineralogy, 8, 349–354.

Brunet, F., Chopin, C., and Seifert, F. (1998) Phase relations in the MgO-P_2O_5-H_2O system and the stability of phosphoellenbergerite: petrological implications. Contributions to Mineralogy and Petrology, 131, 54–70.

Brush, G.J. and Dana, E.S. (1879) On the mineral locality of Fairfield County, Connecticut, with the description of two additional new species. American Journal of Science, 117, 359–368.

——— (1890) On the mineral locality of Fairfield County, Connecticut: Fifth paper. American Journal of Science, 139, 201–216.

Carson, C.J., Hand, M., and Dirks, P.H.G.M. (1995) Stable coexistence of grandidierite and kornerupine during medium pressure granulite facies metamorphism. Mineralogical Magazine, 59, 327–339.

Carson, C.J., Powell, R., Wilson, C.J.L., and Dirks, P.H.G.M. (1997) Partial melting during tectonic exhumation of a granulite terrane: an example from the Larsemann Hills, East Antarctica. Journal of metamorphic Geology, 15, 105–126.

Černý, P., Selway, J.B., Ercit, T.S., Breaks, F.W., Anderson, A.J., and Anderson, S.D. (1998) Graftonite—beusite in granitic pegmatites of the Superior Province: A study in contrasts. Canadian Mineralogist, 36, 367–376.

Cesare, B., Cruciani, G., and Russo, U. (2003) Hydrogen deficiency in Ti-rich biotite from anatectic metapelites (El Joyazo, SE Spain): Crystal-chemical aspects and implications for high-temperature petrogenesis. American Mineralogist, 88, 583–595.

Charalampides, G., Ericsson, T., Nord, A.G., and Khangi, F. (1988) Studies of hydrothermally prepared $(Fe,M)_3(PO_4)_2$-sarcopsides. Neues Jahrbuch für Mineralogie Monatshefte, 1988, 324–336.

Corbella i Cordomí, M. and Melgarejo i Draper, J.-C. (1990) Características y distribución de los fosfatos de las pegmatitas graníticas de la peninsula del Cap de Creus (Pirineo oriental catalán). Boletín de la Sociedad Española de Mineralogía, 13, 169–182.

Dirks, P.H.G.M., Carson, C.J., and Wilson, C.J.L. (1993) The deformation history of the Larsemann Hills, Prydz Bay: the importance of the Pan-African (500 Ma) in East Antarctica. Antarctic Science, 5, 179–192.

Domanskii, A.I., Smolin, Yu.I., Shepelev, Yu.F., and Majling, J. (1983) Determination of crystal structure of triple magnesium calcium sodium orthophosphate $Mg_{21}Ca_4Na_4(PO_4)_{18}$. Soviet Physics, Crystallography, 27, 535–537.

Fisher, D.J. (1965) Dickinsonites, fillowite, and alluaudites. American Mineralogist, 50, 1647–1669.

Fitzsimons, I.C.W. (1996) Metapelitic migmatites from Brattstrand Bluffs, East Antarctica—Metamorphism, melting, and exhumation of the mid crust. Journal of Petrology, 37, 395–414.

Floss, C. (1999) Fe,Mg,Mn-bearing phosphates in the GRA 95209 meteorite: Occurrences and mineral chemistry. American Mineralogist, 84, 1354–1359.

——— (2000) Complexities on the acapulcoite-lodranite parent body: Evidence from trace-element distributions in silicate minerals. Meteoritics and Planetary Science, 35, 1073–1085.

Fransolet, A.-M. and Schreyer, W. (1981) Unusual, iron-bearing apatite from a garnetiferous pegmatoid, Northampton Block, Western Australia. Neues Jahrbuch für Mineralogie Monatshefte, 1981, 317–327.

Fransolet, A.-M., Fontan, F., Keller, P., and Antenucci, D. (1998) La série johnsomervilleïte-fillowite dans les associations de phosphates de pegmatites granitiques de l'Afrique Centrale. Canadian Mineralogist, 36, 355–366

Gnos, E. and Kurz, D. (1994) Sapphirine-quartz and sapphirine-corundum assemblages in metamorphic rocks associated with the Semail Ophiolite (United Arab Emirates). Contributions to Mineralogy and Petrology, 116, 398–410.

Harley, S. (1998) On the occurrence and characterization of ultrahigh-temperature crustal metamorphism. In P.J. Treloar and P.J. O'Brien, Eds., What Drives Metamorphism and Metamorphic Reactions?, 138, p. 81–107. Special Publications, Geological Society, London.

Harlov, D.E. and Förster, H.-J. (2002) High-grade fluid metasomatism on both a local and regional scale: the Seward Peninsula, Alaska, and the Val Strona di Omegna, Ivrea-Verbano Zone, Northern Italy. Part II: Phosphate mineral chemistry. Journal of Petrology, 43, 801–824.

Harlov, D., Renzulli, A., and Ridolfi, F. (2006) Iron-bearing chlor-fluorapatites in crustal xenoliths from the Stromboli volcano, (Aeolian Islands, Southern Italy): an indicator of fluid processes during contact metamorphism. European Journal of Mineralogy, 18, 233–241.

Hatert, F. (2002) Cristallochimie et synthèse hydrothermale d'alluaudites dans le système Na-Mn-Fe-P-O: contribution au problème de la genèse de ces phosphates dans les pegmatites granitiques, 247 p. Ph.D. thesis, University of Liège, Belgium.

Hatert, F. and Fransolet, A.-M. (2003) Preliminary data on the crystal chemistry of synthetic fillowite-type phosphates. Berichte der Deutschen Mineralogischen Gesellschaft, Beihefte zum European Journal of Mineralogy, 15(1), 76.

——— (2004) The stability of alluaudite in granitic pegmatites. Geological Society of America Abstracts with Programs, 36(5), 115.

Heming, R.F. and Carmichael, I.S.E. (1973) High-temperature pumice flows from Rabaul Caldera Papua, New Guinea. Contributions to Mineralogy and Petrology, 38, 1–20.

Holdaway, M.J. and Lee, S.M. (1977) Fe-Mg cordierite stability in high-grade pelitic rocks based on experimental, theoretical, and natural observations. Contributions to Mineralogy and Petrology, 63, 175–198.

Kapustin, Yu.L. (1987) The composition of apatite from metamorphic rocks. Geochemistry International, 24(4), 45–51.

Keller, P., Lissner, F., Hatert, F., and Schleid, T. (2001) $Na_4(Na,Mn)_4Mn_{22}(PO_4)_{18}$, eine isotype Verbindung der Fillowit-Johnsomervilleit-Reihe. Zeitschrift für Kristallographie, Supplement issue 18, 150.

Livingstone, A. (1980) Johnsomervilleite, a new transition-metal phosphate mineral from Loch Quoich area, Scotland. Mineralogical Magazine, 43, 833–836.

London, D. (1992) Phosphorus in S-type magmas: The P_2O_5 content of feldspars from peraluminous granites, pegmatites, and rhyolites. American Mineralogist, 77, 126–145.

——— (1998) Phosphorus-rich peraluminous granites. Acta Universitatis Carolinae-Geologica, 42, 64–68.

London, D. and Burt, D.M. (1982) Alteration of spodumene, montebrasite, and lithiophilite in pegmatites of the White Picacho District, Arizona. American Mineralogist, 67, 97–113.

London, D., Černý, P., Loomis, J.L., and Pan, J.J. (1990) Phosphorus in alkali feldspars of rare-element granitic pegmatites. Canadian Mineralogist, 28, 771–786.

London, D., Wolf, M.B., Morgan, G.B., VI, and Garrido, M.G. (1999) Experimental silicate-phosphate equilibria in peraluminous granitic magmas, with a case study of the Alburquerque Batholith at Tres Arroyos, Badajoz, Spain. Journal of Petrology, 40, 215–240.

Ma, Z., Shi, N., and Ye, D. (2005) Mineralogy and crystal structure determination of Mg-fillowite. Science in China Series D Earth Sciences, 48, 635–646.

Mandarino, J.A. (1981) The Gladstone-Dale relationship: Part IV. The compatibility concept and its application. Canadian Mineralogist, 19, 441–450.

McCoy, T.J., Steele, I.M., Keil, K., Leonard, B.F., and Endress, M. (1994) Chladniite, $Na_2CaMg_7(PO_4)_6$: A new mineral from the Carlton (IIICD) iron meteorite. American Mineralogist, 79, 375–380.

McCoy, T.J., Carson, W.D., Nittler, L.R. Stroud, R.M. Bogard, D.D., and Garrison, D.H. (2006) Graves Nunataks 95209: A snapshot of metal segregation and core formation. Geochimica and Cosmochimica Acta, 70, 516–531.

Medenbach, O. (1986) Ein modifiziertes Kristallbohrgerät nach Verschure (1978) zur Isolierung kleiner Einkristalle aus Dünnschliffen. Fortschritte der Mineralogie, Beiheft, 64(1), 113.

Merlet, C. (1994) An accurate computer correction program for quantitative electron-probe microanalysis. Mikrochimica Acta, 114, 363–376.

Moore, P.B. (1989) Perception of structural complexity: Fillowite revisited and α-iron related. American Mineralogist, 74, 918–926.

Olsen, E.J. and Steele, I.M. (1997) Galileiite: A new meteoritic phosphate mineral. Meteoritics and Planetary Science, 32 (Supplement), A155–A156.

Olsen, E.J., Kracher, A., Davis, A.M., Steele, I.M., Hutcheon, I.D., and Bunch, T.E. (1999) The phosphates of IIIAB iron meteorites. Meteoritics and Planetary Science, 34, 285–300.

Pan, Y. and Fleet, M.E. (2002) Compositions of the apatite-group minerals: Substitution mechanisms and controlling factors. In M.J. Kohn, J. Rakovan, and J. M. Hughes, Eds., Phosphates: Geochemical, Geobiological, and Materials Importance, 48, p. 13–49. Reviews in Mineralogy and Geochemistry, Mineralogical Society of America, Chantilly, Virginia.

Pattison, D.R.M. (1992) Stability of andalusite and sillimanite and the Al_2SiO_5 triple point: Constraints from the Ballachulish aureole, Scotland. Journal of Geology, 100, 423–446

Povondra, P. (1992) Crystal chemistry of rock-forming apatites from the Bohemian Massif. Acta Universitatis Carolinae-Geologica, 36, 197–224.

Povondra, P. and Vrána, S. (1993) Crystal chemistry of apatite in tourmaline-bearing alkali-feldspar orthogneiss near Hluboká nad Vltavou, southern Bohemia. Journal of the Czech Geological Society, 38, 165–170.

Ren, L., Grew, E.S., Xiong, M., and Ma, Z. (2003) Wagnerite-*Ma5bc*, a new polytype of $Mg_2(PO_4)(F,OH)$, from granulite-facies paragneiss, Larsemann Hills, Prydz Bay, East Antarctica. Canadian Mineralogist, 41, 393–411.

Ren, L., Grew, E.S., Xiong, M., and Wang, Y. (2005) Petrological implication of wagnerite-*Ma5bc* in the quartzofeldspathic gneiss, Larsemann Hills, East Antarctica. Progress in Natural Science, 15, 523–529.

Sheldrick, G.M. (1993) SHELXL93: Program for crystal structure determination. University of Göttingen, Germany.

Spear, F.S. and Pyle, J.M. (2002) Apatite, monazite, and xenotime in metamorphic rocks. In M.J. Kohn, J. Rakovan, and J. M. Hughes, Eds., Phosphates: Geochemical, Geobiological, and Materials Importance, 48, p. 293–335. Reviews in Mineralogy and Geochemistry, Mineralogical Society of America, Chantilly, Virginia.

Stevens, G., Clemens, J.D., and Droop, G.T.R. (1997) Melt production during granulite-facies anatexis: experimental data from "primitive" metasedimentary protoliths. Contributions to Mineralogy and Petrology, 128, 352–370.

Strunz, H. and Nickel, E.H. (2001) Strunz Mineralogical Tables. Chemical-Structural Mineral Classification System, 9th edition. Schweizerbart, Stuttgart.

Stüwe, K., Braun, H.-M., and Peer, H. (1989) Geology and structure of the Larsemann Hills area, Prydz Bay, East Antarctica. Australian Journal of Earth Sciences, 36, 219–241.

Sugiura, N. and Hoshino, H. (2003) Mn-Cr chronology of five IIIAB iron meteorites. Meteoritics and Planetary Science, 38, 117–143.

Thost, D.E., Hensen, B.J., and Motoyoshi, Y. (1994) The geology of a rapidly uplifted medium and low-pressure granulite facies terrane of Pan-African age: the Bolingen Islands, Prydz Bay, Eastern Antarctica. Petrology, 2, 293–316.

Tong, L. and Liu X. (1997) The prograde metamorphism of the Larsemann Hills, East Antarctica: Evidence for an anticlockwise *P-T* path. In C.A. Ricci, Ed., The Antarctic Region: Geological Evolution and Processes; Proceedings of the 7th International Symposium on Antarctic Earth Sciences, Siena, 1995, p. 105–114. Terra Antartica, Siena, Italy.

Vielzeuf, D. and Holloway, J.R. (1988) Experimental determination of the fluid-absent melting relations in the pelitic system: consequences for crustal differentiation. Contributions to Mineralogy and Petrology, 98, 257–276.

Walenta, K. and Theye, T. (2005) Plumboagardite, a new mineral of the mixite group from an occurrence in the Southern Black Forest, Germany. Neues Jahrbuch für Mineralogie Abhandlungen, 181, 219–222.

White, R.W. and Powell, R. (2002) Melt loss and the preservation of granulite facies mineral assemblages. Journal of Metamorphic Geology, 20, 621–632.

Wolf, M.B. and London, D. (1994) Apatite dissolution into peraluminous haplogranitic melts: An experimental study of solubilities and mechanisms. Geochimica et Cosmochimica Acta, 58, 4127–4145.

MANUSCRIPT RECEIVED JANUARY 26, 2006
MANUSCRIPT ACCEPTED APRIL 17, 2006
MANUSCRIPT HANDLED BY SERGEY KRIVOVICHEV